Asian Journal of Chemistry; Vol. 36, No. 6 (2024), 1348-1358

ASIAN JOURNAL OF CHEMISTRY

https://doi.org/10.14233/ajchem.2024.31336

Multifunctional Transition Metal Complexes: Design, Synthesis, Luminescent Features, Electrical Behaviour, Nanostructure Morphology and Bioactive Properties with 1,1-Dicyanoethylene-2,2-dithiolate and *p*-Phenylenediamine Ligands

ARIJIT DAS[1,*], SYED ARSHAD HUSSAIN[2], HRITINAVA BANIK[2], DEBASISH MAITI[3], TAMANNA AKTAR[3], SANDEEP ACHARYA[4] and PARESH DEBNATH[1,5,*]

[1]Department of Chemistry, Bir Bikram Memorial College, Agartala-799004, India
[2]Thin Film and Nanoscience Laboratory, Department of Physics, Tripura University, Suryamaninagar-799022, India
[3]Department of Human Physiology, Tripura University, Agartala-799022, India
[4]Department of Botany, R.K. Mahavidyalaya, Kailashahar, Unakoti-799277, India
[5]Department of Chemistry, National Institute of Technology Agartala, Jirania-799046, India

*Corresponding authors: E-mail: arijitdas78chem@gmail.com; pareshchem1990@gmail.com

Received: 4 February 2024; *Accepted*: 20 April 2024; *Published online*: 31 May 2024; AJC-21648

Four new transition metal complexes (**1**-**4**) were successfully synthesized through the reaction of $M(NO_3)_2{\cdot}nH_2O$ (M = Ni, Co, Cd or Zn; n = 6 for Ni, Co, Zn; n = 4 for Cd) with 1,1-dicyanoethylene-2,2-dithiolate (*i*-MNT^{2-}) and *p*-phenylenediamine (PPD) ligands. The synthesized metal complexes were characterized by CHN-analysis, electronic, FTIR and ^{1}H NMR spectroscopic techniques. The electronic transition investigations reveals six coordinate octahedral geometry for Ni(II), distorted octahedral for Co(II), four coordinate tetrahedral geometry for Cd(II) and Zn(II) complexes. All the four metal complexes displayed a significant red shift in the absorption maximum, suggesting their successful assembly. The luminescence behaviour exhibited the prominent fluorescence within the visible range. The current-voltage characteristics revealed that complexes **2** and **3** exhibited ohmic behaviour, displaying a linear curve. On the other hand, complexes **1** and **4** initially maintained a low conducting state (OFF state) until a specific voltage threshold (V_{Th}), beyond which the current sharply increased, transitioning to a higher current state (ON state). The FESEM images of the metal complexes strongly indicated a nano-scale aggregated structure. In terms of antibacterial activity, complexes **3** and **4** demonstrated promising efficacy against various bacterial strains, with complex **3** being particularly potent. The fungicidal activity of all four metal complexes was remarkable against *Magnaporthe grisea*, *Cochliobolus miyabeanus* and *Synchitrium endobioticum*, however, no fungicidal activity was found against *Trichophyton mentagrophytes* and *Candida albicans*.

Keywords: Metal complexes, 1,1-Dithiolates, *p*-Phenylenediamine, Antibacterial activity, Antifungal activity.

INTRODUCTION

Transition metal mixed ligand complexes containing 1,1-dithiolate ligand has immense attention to researcher because of their versatile structures and applications. The 1,1-dithiolate ligand such as 1-cyano-1-carboethoxyethylene-2,2-dithiolate (CED^{2-}) and *iso*-maleonitrile dithiolate (*i*-MNT^{2-}) form several nickel complexes with secondary ligands that are nitrogen donor ligands *e.g.* pyridine, *o*-phenylenediamine, β-picoline, γ-picoline or α-picoline [1,2]. The ligand *i*-MNT^{2-} also form a variety of crown ether complexes with 18-crown-6, benzo-15-crown-6, naphtho-15-crown-5, *etc.* which consists of two [K-benzo15-crown-5]$^+$, [K18-crown-6]$^+$ or $[Na_{18}\text{-crown-}_6]^+$ or type cations and one $[M(i\text{-mnt})_2]^-$ anions [3-7]. Another significant type of complex is ion-pair complex, $[Cation]_2[M(i\text{-mnt})_2]$ where cationic part is not coordinated to M-centre but exist as ion-pair and M-centre adopted square-planar coordination geometry [8-10]. There are reports in the literature of clusters with a Cu_8/Ag_8 core that have a unique tetracapped tetrahedral structure that are contained in cyclic hydrides where six *i*-MNT ligands work together to form an S_{12} icosahedron that envelops this core. According to the findings, these ligands form a tetrametallic-tetraconnective (μ_2-μ_2) bonding mode [11,12]. Further, the complexes of mixed ligand containing 1,1-dicyanoethylene-

2,2-dithiolates also showed diverse structures [13-16]. Recent studies shows that dithiolate ligands have rigid structures, forms homoleptic complexes and also have highly efficient thermally activated delayed fluorescence in carbene zinc(II) dithiolates [17-19].

The study invetigated extensively into the reactivity of zinc(II) salts upon exposure to 1,3-diaminopropane (dap) and K_2(*i*-MNT). This investigation took place in the presence of two distinct *N*-donor ligands *viz*. α-picoline (2-methylpyridine) and γ-picoline (4-methylpyridine) [14]. The outcome of this study yielded two distinct Zn(II) coordination complexes. The first complex exhibits a dimeric structure that displays a unique arrangement of its individual components, while the second complex displays an intriguing polymeric structure indicating a significant deviation from the first complex [14]. In addition to structural chemistry, 1,1-dithiolate complexes also exhibits host–guest properties [20], catalytic properties [21], *etc*. The biological investigations of these mixed ligand 1,1-dithiolate complexes is reported in the literature recently, which includes antifungal activities [22-25], antibacterial, cytotoxic activities [26,27], *etc*.

In view of literature survey, we are interested to synthesize mixed ligand complexes of 1,1-dithiolate ligand with few transition metals which could show potential antibacterial and antifungal activities. As a result, we present here the synthesis, structural characterization, luminescent properties, current-voltage characteristics, FESEM studies, antibacterial and antifungal activity of transition metal complexes of Ni, Co, Cd and Zn with 1,1-dicyanoethylene-2,2-dithiolate and *p*-phenylenediamine.

EXPERIMENTAL

The chemicals *viz*. *p*-phenylenediamine (PPD), $Ni(NO_3)_2·6H_2O$, $Co(NO_3)_2·6H_2O$, $Cd(NO_3)_2·4H_2O$ and $Zn(NO_3)_2·6H_2O$ were procured from Sigma-Aldrich and used without additional purification. The synthesis of K_2*i*-MNT·H_2O followed a reported literature procedure [28]. Nutrient Agar (Hi-media) served as the culture medium for the bacterial species growth. Elemental analysis (C, H, N) was conducted using a Perkin-Elmer 2400 series II instrument. Infrared (IR) absorption bands for both the ligand and the complex were recorded in 4000–400 cm^{-1} range using a Bruker Alpha II-E spectrophotometer. The UV-Vis absorption spectra of the complexes were measured in DMSO solvent within 250-800 nm range using a Shimadzu UV-1800 spectrophotometer. Fluorescence observations were made with a Perkin-Elmer LS 55 fluorescence spectrophotometer. The ^{1}H NMR spectra of the complex were obtained at 400 MHz on a Bruker AMX 400 spectrometer instrument, with Me_4Si as the reference compound. The FESEM images were obtained using the FESEM Sigma 300 model from Zeiss Pvt. Ltd. operating at a 5 kV acceleration voltage. Thin films of the metal complexes were prepared on ITO-coated glass substrates (resistivity 15–25 Ω/Sq) and electrical characterizations were performed using a Sourcemeter Kiethley-2614 B and a Probe station Everbeing C2.

Synthesis of [Ni(PPD)$_2$(*i*-MNT).2H$_2$O] complex (1): In brief, 0.7269 g (2.5 mmol) of $Ni(NO_3)_2·6H_2O$ was miexed in 25 mL distilled water and stirred. To this solution, 25 mL ethanolic solution containing 0.54 g (5 mmol) of *p*-phenylenediamine (PPD) was slowly added with continuous stirring, resulting in a noticeable change in colour from light green to a deep green colour. Subsequently, 25 mL aqueous solution containing 0.59 g (2.5 mmol) of K_2(*i*-MNT)·H_2O was added gradually to the mixture while stirring. Initially, a yellow precipitate formed, converting into a brown colour over 10 min. Even after an additional 45 min of stirring, the brown precipitate persisted. The formed brown precipitate was isolated by filtration using Whatman no. 41 filter paper (**Scheme-I**). The collected precipitate underwent sequential washing with water, ethanol and acetone to eliminate impurities. Following the washings, the precipitate was subjected to suction and then dried under vacuum conditions using $CaCl_2$ in a desiccator. Yield: 0.84 g, 75%; Anal. calcd. (found) % for $C_{16}H_{18}N_6O_2S_2Ni$: C, 42.78 (42.38); H, 4.04 (4.15); N, 18.71 (18.41). UV-visible (DMSO) λ_{max} (nm): 264, 340, 456, 637. IR (KBr, cm^{-1}): 3435br, 3297s ν(N-H *str.*)/ν(N-H *str.*) + ν(O-H *str.*), 2230vs ν(C≡N *str.*),

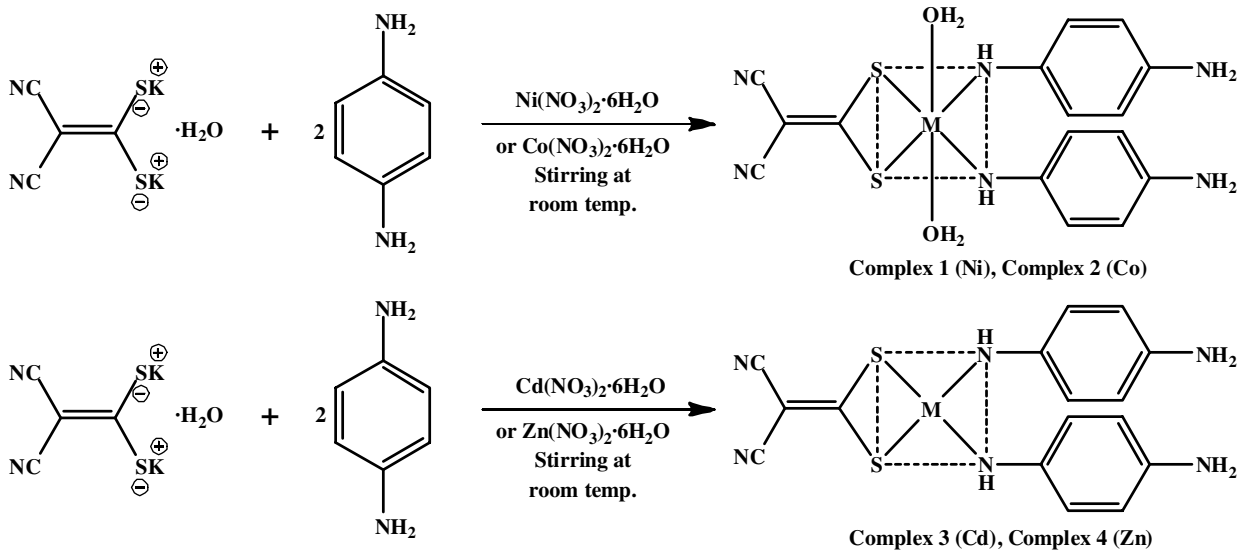

Scheme-I: Reaction scheme for the synthesis of complexes **1**, **2**, **3** and **4**

1389vs ν(C=C), 1073s, 1033s ν_{as}(=CS_2), 943s ν_s(=CS_2), 903s ν(C-S *str.*).

Synthesis of [Co(PPD)$_2$(*i*-MNT).2H$_2$O] complex (2): $Co(NO_3)_2 \cdot 6H_2O$ (0.7275 g, 2.5 mmol) was dissolved in 25 mL distilled water and stirred. Similar procedure was followed as in case of Ni-complex **1**. Yield: 0.93 g, 82%; Anal. calcd. (found) % for $C_{16}H_{18}N_6O_2S_2Co$: C, 42.76 (42.65); H, 4.04 (4.20); N, 18.70 (18.75). UV-visible (DMSO) λ_{max} (nm): 338, 376, 413. IR (KBr, cm^{-1}): 3435br, 3362s ν(N-H *str.*)/ν(N-H *str.*) + ν(O-H *str.*), 2198vs ν(C≡N *str.*), 1362s ν(C=C), 1170s, 1131s ν_{as}(=CS_2), 949s ν_s(=CS_2),899s ν(C-S *str.*).

Synthesis of [Cd(PPD)$_2$(*i*-MNT)] complex (3): $Cd(NO_3)_2 \cdot 4H_2O$ (0.771 g, 2.5 mmol) was dissolved in 25 mL distilled water and stirred. Similar procedure was followed as in case of Ni-complex **1**. Yield: 0.86 g, 74%; Anal. calcd. (found) % for $C_{16}H_{14}N_6S_2Cd$: C, 41.16 (41.07); H, 3.02 (3.13); N, 18.00 (18.31). UV-visible (DMSO) λ_{max} (nm): 311, 340. IR (KBr, cm^{-1}): 3348m, 3279s ν(N-H *str.*)/ν(N-H *str.*) + ν(O-H *str.*), 2198vs ν(C≡N *str.*), 1396vs, 1374vs ν(C=C), 1030s, 1033s ν_{as}(=CS_2), 946s ν_s(=CS_2), 931m ν(C-S *str.*).^{1}H NMR (DMSO-d_6, 400 MHz) δ_H, ligand skeleton(PPD ligand): 6.39 (s, 8H, Ar-H), 4.32 (s, 2H, N-H (br) of N-Cd), 3.37 [s, 4H, N-H (br) of -NH_2] ppm.

Synthesis of [Zn(PPD)$_2$(*i*-MNT)] complex (4): $Zn(NO_3)_2 \cdot 6H_2O$ (0.743 g, 2.5 mmol) was dissolved in 25 mL distilled water and stirred. Similar procedure was followed as in case of Ni-complex **1**. Yield: 0.75 g, 71%; Anal. calcd. (found) % for $C_{16}H_{14}N_6S_2Zn$: C, 45.77 (45.68); H, 3.31 (3.24); N, 20.02 (20.12). UV-visible (DMSO) λ_{max} (nm): 261, 305, 334. IR (KBr, cm^{-1}): 3378m, 3309s ν(N-H *str.*)/ν(N-H *str.*) + ν(O-H *str.*), 2221vs ν(C≡N *str.*), 1381s ν(C=C), 1130w, 1080s ν_{as}(=CS_2), 957s ν_s(=CS_2), 883s ν(C-S *str.*). ^{1}H NMR (DMSO-d_6, 400 MHz) δ_H, ligand skeleton (PPD ligand): 6.44 (m, 8H, Ar-H), 4.63 (s, 2H, N-H (br) of N-Zn), 3.40 (s, 4H, N-H (br) of -NH_2) ppm.

Antibacterial assay: The antibacterial efficacy of K_2(*i*-MNT)·H_2O, along with complexes **1**-**4**, was assessed against pathogenic Gram-negative *Escherichia coli*, *Shigella boydii* and Gram-positive *Staphylococcus aureus* bacteria using the zone of inhibition (ZOI) method [29]. Additionally, the antibacterial activity of standard antibiotics, gentamycin and polymyxin B, specific to the bacterial strains, was tested as positive controls. Overnight cultures of bacterial strains were inoculated onto nutrient agar plates, forming a complete lawn. Four discs were gently pressed onto each plate using sterile forceps. One disc, serving as blank control consist of 4 µL of distilled water, while the remaining three discs were loaded with drugs at concentrations of 100, 10 and 1 µg/disc. The Petri dishes were then incubated for 24 h in a 37 ºC incubator. After overnight incubation, a distinct zone of inhibition was observed around the active compound and the diameter of this zone was measured (in mm). Statistical analysis was performed using Student's T test to assess the significance of the results.

Antifungal activity: The antifungal efficacy of K_2(*i*-MNT)·H_2O ligand and its metal complexes was assessed using the disc diffusion method [30,31]. A comparison was prepared with the standard griseofulvin (10 µg/disc). Fungal strains were cultivated on Sabouraud dextrose agar. In the standard disc diffusion procedure, a 20% (w/v) stock solution of each dry extract (both complex and its primary ligand) was prepared in pure DMSO. For molds, the mature spore suspensions were obtained by gently washing the solid media surface with a 0.05% (v/v) Tween 80 solution and the resulting suspension was adjusted to 10^6 spores/mL. Whatman No. 4 filter paper discs (6 mm diameter) were placed on the inoculated agar surfaces and saturated with 15 µL of stock solutions. Positive controls utilized griseofulvin (10 µg/disc) discs, while pure DMSO (15 µL) served as the negative control. Mold growth on the plates was assessed after 96 h at 25 ºC. All the readings were based on 5 replicates.

RESULTS AND DISCUSSION

Four novel transition metal complexes (**1**-**4**) were successfully synthesized by reacting metal(II) salts (M = Ni, Co, Cd or Zn), *p*-phenylenediamine and 1,1-dicyanoethylene-2,2-dithiolate (*i*-MNT^{2-}) ligands in a molar ratio of 1:2:1 for in a solvent mixture of methanol and water. Remarkably, these newly synthesized complexes exhibit significant solubility across a wide range of organic solvents.

Weight loss experiment: To perform the weight loss experiments for the four synthesized complexes, 4 h of heating a small volume of material in a glass tube at 100, 120, 150 and 180 ºC electric oven was used. Between 150 and 180 ºC, two complexes **1** and **2** exhibit weight decreases which is consistent with two coordinated water molecules.

Electronic absorption spectra: The electronic absorption spectra of the four synthesized metal(II) complexes were analyzed both in DMSO solution and when assembled into thin films. The corresponding spectra are depicted in Figs. 1 and 2, respectively. The molar concentrations of all the complexes in solution were taken very low in order to avoid aggregation. The absorption spectra of Ni(II) complex (complex **1**) exhibits two characteristic bands fall in the visible region at 637 nm and 456 nm assignable to $^3A_{2g} \rightarrow {}^3T_{1g}$ (F) and $^3A_{2g} \rightarrow {}^3T_{1g}$ (P) suggesting the octahedral coordination around Ni(II). Cobalt(II) complex (complex **2**) exhibits two characteristic bands at 413 nm (visible) and 376 nm (near visible) assignable to $^4T_{1g}$(F) $\rightarrow {}^4T_{1g}$(P) suggesting six coordinated Co(II) geometry. It also falls in the region of low spin and the square planar Co(II) geometry involving transitions from xz, yz$\rightarrow z^2$ and x^2-$y^2 \rightarrow z^2$. This can conclude that complex **2** exhibits distorted octahedral stereochemistry around Co(II) [32,33]. The band at 413 nm is not distinct at lower concentration but appears as distinct band at higher concentration. In the absorption spectra of complex **3** solutions, a significant peak appears at 340 nm, accompanied by a faint curve at 311 nm. Conversely, the absorption spectra of complex **4** solutions exhibit two prominent peaks at 334 nm and 305 nm, along with a subdued curve at 261 nm. Notably, no *d*–*d* transition is anticipated for Cd(II) and Zn(II) complexes. In both complexes, individual coordination of two PPD nitrogen atoms and thiolate ions coordination to Cd(II) and Zn(II) with identical constituents occur. These findings suggest an auxochromic shift of N–atom in PPD for both Cd(II) and Zn(II) complexes. Consequently, the UV-Vis transition analyses support the proposed octahedral geometry for Ni(II),

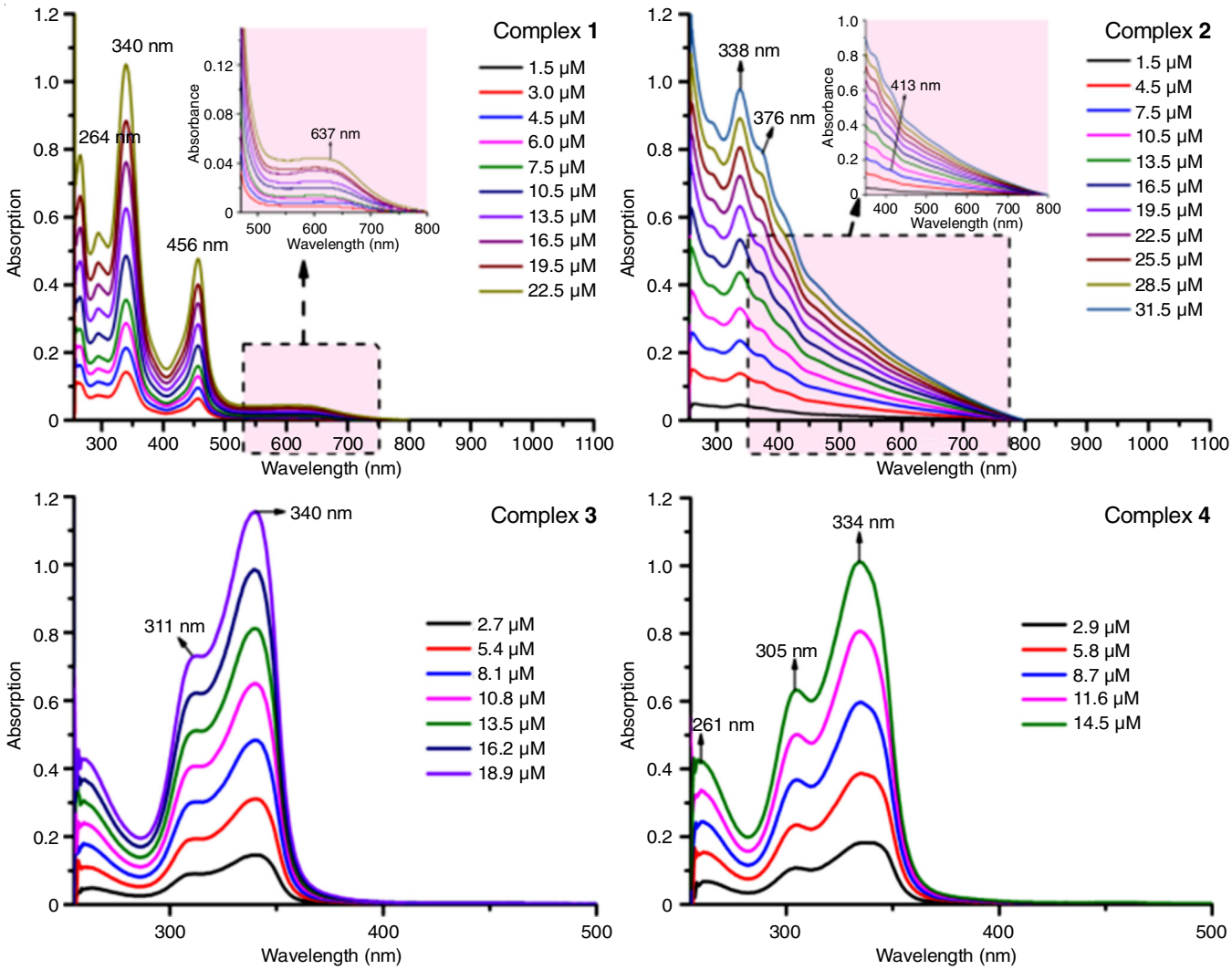

Fig. 1. UV-Vis absorption spectra in DMSO solution for complexes **1**, **2**, **3** and **4**

distorted octahedral for Co(II) and tetrahedral geometry for Cd(II) and Zn(II) complexes.

For real practical device applications, it is a prerequisite to assemble the designed molecules in the constrained geometry of ultrathin films. Also, it has been seen that the optoelectronics behaviours of the molecules are largely affected when they are confined within the restricted geometry of nano- to micro-scale thin films [34]. Accordingly, all the four designed complexes have been assembled onto thin films and their absorption behaviour have been investigated. Interestingly for all the complexes, marked red shift of the absorption maximum compared to that in solution has been observed. In some cases, certain weak curves that were observed in the absorption spectra of the solution are not observed in their corresponding thin film counterpart. It may be mentioned in this context that overlapping of energy levels as well aggregation of molecules occurred when they are incorporated into thin films leading to changes in the spectral behaviour [35]. For different compounds, thin film absorption spectra showed significant changes in intensity and red shifting order. This may be due to the difference in order of association or aggregation as well as ordering of molecules in thin films for four different complexes [36].

Fluorescence study: The investigations revealed that all the four complexes synthesized in the present study showed the prominent fluorescence behaviour within visible ranges. Corresponding spectra are shown in Fig. 3. Complex **1** showed strong fluorescence at 410 and 582 nm for excitation wavelength 340 and 456 nm, respectively. Complex **2** showed fluorescence bands at 408 and 444 nm for excitation wavelength 338 and 376 nm respectively. Complexes **3** and **4** showed prominent fluorescence at 409 and 411 nm with excitation wavelength 340 and 334 nm, respectively. Interestingly, it has been observed that the fluorescence behaviour of complexes **1** and **2** were largely dependent on the excitation wavelength, whereas, the fluorescence of the other two complexes was independent of excitation wavelength. These results clearly indicate that all the four metal complexes may be suitable for photochemical applications. Also, the fluorescence behaviour of the first two complexes may be tuned by varying the excitation wavelength.

IR spectroscopy: Fig. 4 illustrates the resonance structure of these complexes, providing a basis for defining *i*-MNT^{2-}. The IR spectra reveal distinct stretching frequencies associated with C≡N, C=C, =CS_2 and C-S from *i*-MNT^{2-} complexes, along with amine vibrations and metal amine nitrogen vibrations

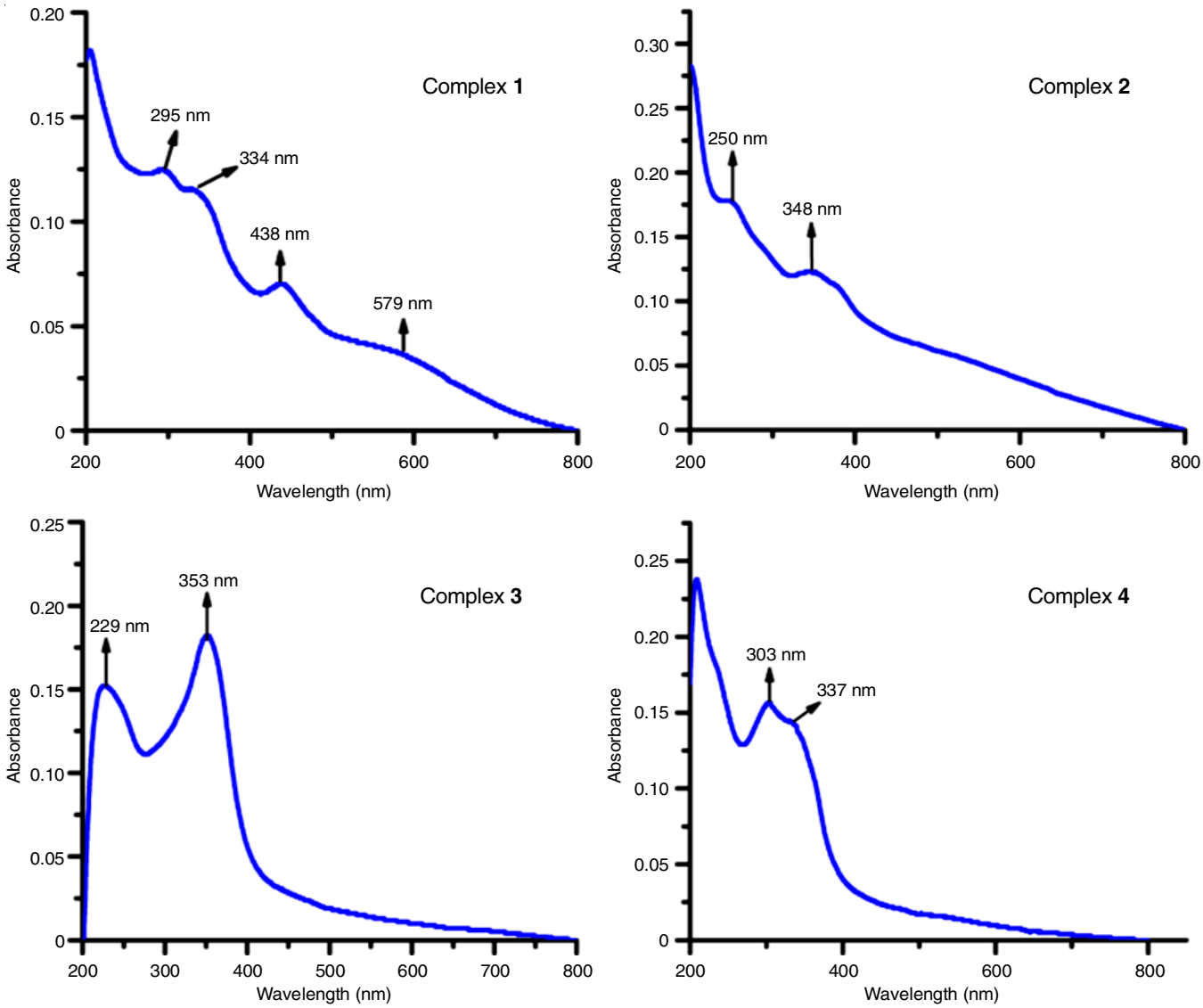

Fig. 2. UV-vis absorption spectra in thin film for complexes **1**, **2**, **3** and **4**

from *p*-phenylenediamine (PPD). The IR spectra of two representative complexes of Ni(II) and Co(II) are presented in Fig. 5. In K_2(*i*-MNT)·H_2O, the ν(C≡N) is observed at 2195 cm^{-1}, with a shoulder at 2200 cm^{-1}, while the four complexes exhibit a sharp absorption in the range of 2230-2198 cm^{-1}. The ν(C=C) absorption in all complexes falls within the range of 1396-1362 cm^{-1}, with a corresponding observation in free K_2(*i*-MNT)·H_2O at 1360 cm^{-1}, suggesting π-electron delocalization out of the C=C bond. Positive shifts in the stretching frequencies of C≡N and C=C support the dominance of resonance form (Fig. 4) in the *i*-MNT^{2-} complexes.

A band at 960 cm^{-1} with a shoulder at 985 cm^{-1} in the IR spectrum of K_2(*i*-MNT)·H_2O, attributed to the =CS_2 group, is found in the range 1170-943 cm^{-1}, whereas the ν(C-S) band of K_2(*i*-MNT)·H_2O at 860 cm^{-1} appears as a single band in the complexes indicating the symmetrical bonding of both sulfurs, consistent with the reported behaviour in K_2(*i*-MNT)·H_2O [37], moreover a single ν(C-S) band is also observed at 900 cm^{-1}. Complexes **1** and **2** exhibit broad bands between 3600-3000 cm^{-1}, attributed to the ν(O-H) and ν(N-H) stretching modes. The ν(N-H) stretching modes from *p*-phenylenediamine (PPD) contribute to a collection of broad bands in the range 3435-3279 cm^{-1}, present in all complexes and even in the dehydrated complexes **1** and **2** at 200 ºC. The ν(N-H) bending (scissoring) vibration mode is observed at 1624-1590 cm^{-1} and 1251-1214 cm^{-1} correspond to the ν(C-N) bending mode in the complexes, while in the PPD ligand, the same mode was observed at 1262 cm^{-1}. The complexes exhibit an out-of-plane C-H ring (aromatic) bending mode, typical of 1,4-disubstituted benzene, with a strong absorption at 842-827 cm^{-1}. Additionally, the ν(C-H) (aromatic ring) resulting from aromatic ligands is observed as weak band(s) in the range of 3141-3021 cm^{-1} in the metal(II) complexes.

NMR spectral studies: The primary focus centered on comparing the ^{1}H NMR profiles of PPD ligand with those of complexes **3** and **4**. This comparative analysis aimed to unravel the coordination behaviour of the ligand within the complexes. The PPD ligand manifests aromatic protons resonating around

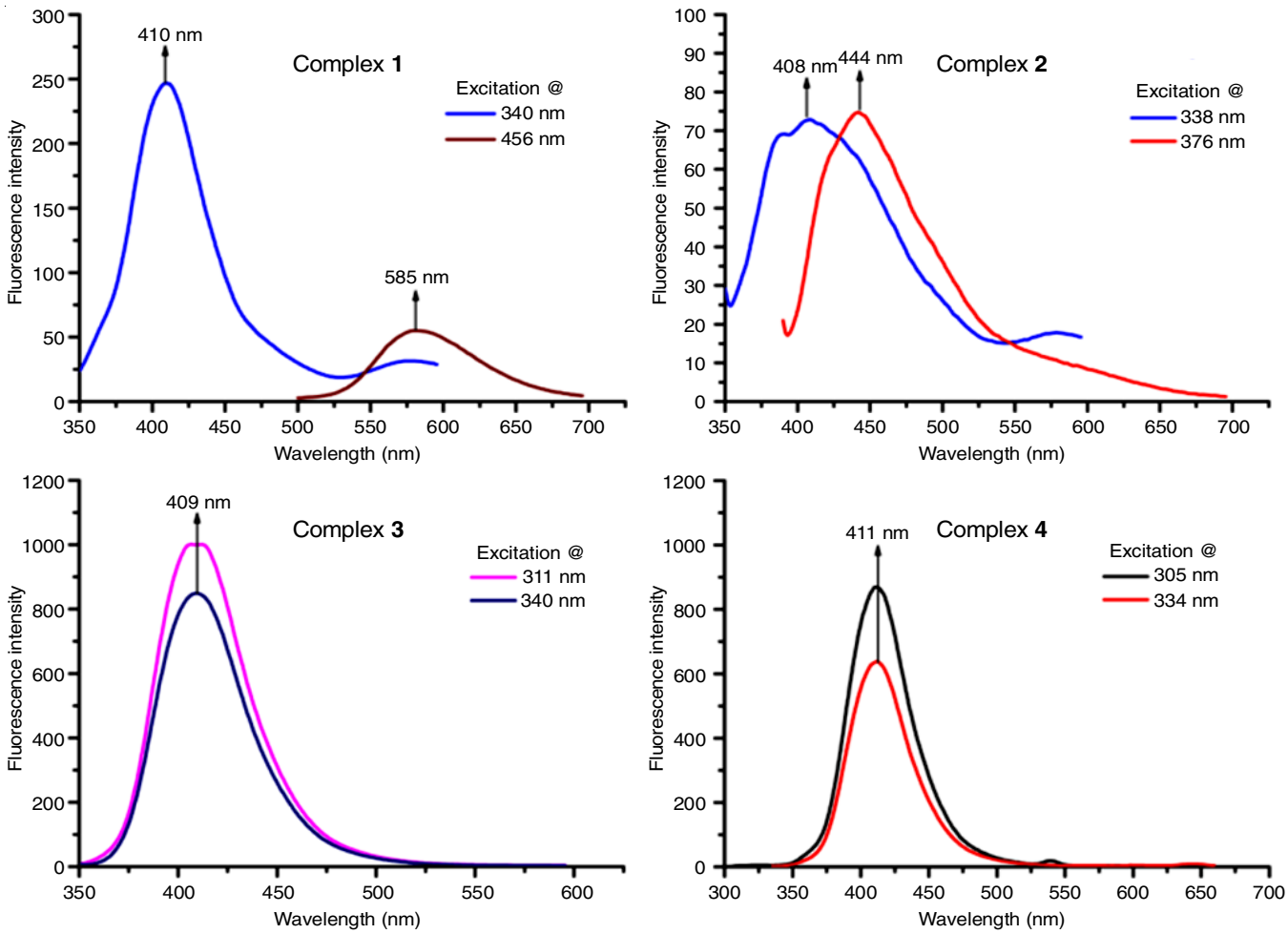

Fig. 3. Fluorescence spectra for complexes **1**, **2**, **3** and **4**

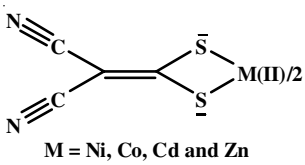

Fig. 4. Dominant resonance forms of *i*-MNT^{2-} complexes

6.55 ppm, while the -NH_2 protons are observed at ~ 3.31 ppm [38]. The aromatic protons in complexes **3** and **4** exhibit a discernible shift in resonance frequency. Specifically, these protons are detected at ~ 6.39 ppm for Cd(II) complex and at ~ 6.44 ppm for the Zn(II) complex (Fig. 6). This shift strongly suggests the involvement of ligand moiety in coordination with

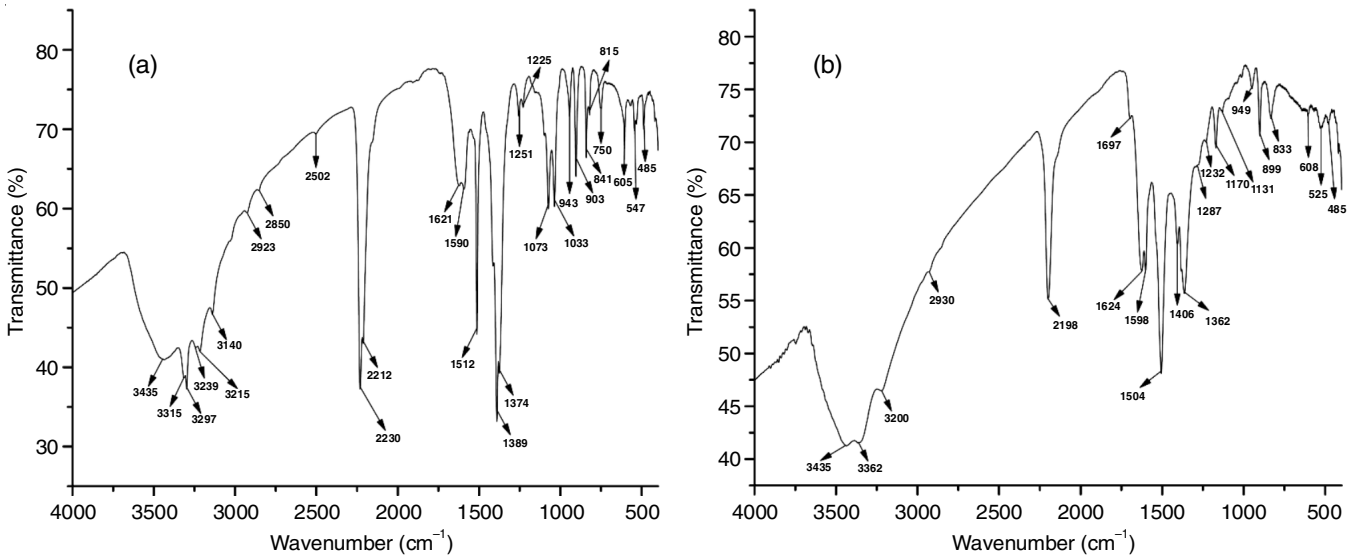

Fig. 5. IR spectrum of (a) Ni(PPD)$_2$(*i*-MNT)·2H$_2$O] complex (**1**) and (b) [Co(PPD)$_2$(*i*-MNT).2H$_2$O] complex (**2**)

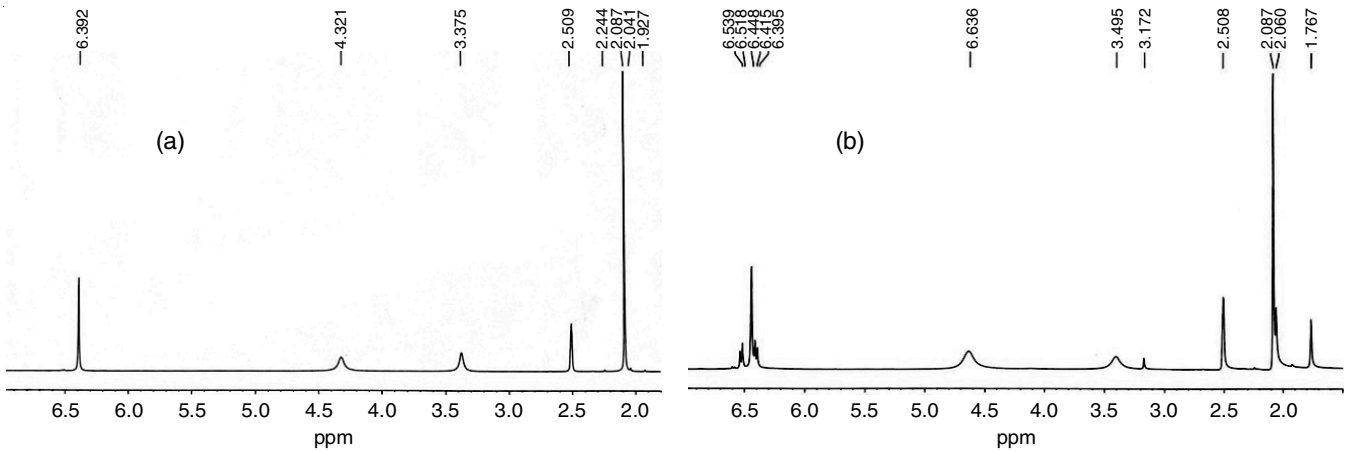

Fig. 6. ^{1}H NMR spectrum of (a) [Cd(PPD)$_2$(*i*-MNT)] complex (**3**) and (b) [Zn(PPD)$_2$(*i*-MNT)] complex (**4**)

the central metal in these complexes. Further examination revealed two distinct N-H signals at δ 3.37 ppm and 4.32 ppm for Cd(II) complex and at δ 3.40 ppm and 4.63 ppm for Zn(II) complex. These findings indicated the coordination of one of the -NH_2 groups with the central metal center, leading to the presence of two N-H signals. This observation provides crucial evidence supporting the coordination of the ligand and offers a deeper understanding of the structural aspects of the complexes.

Current-voltage (I-V) characteristics: Most of the modern electronic devices are based on the current-voltage (I-V) behaviour of the materials. Accordingly, in present study, the I-V characteristics were measured for all the complexes. In order to do that devices with configurations ITO/complex molecules/

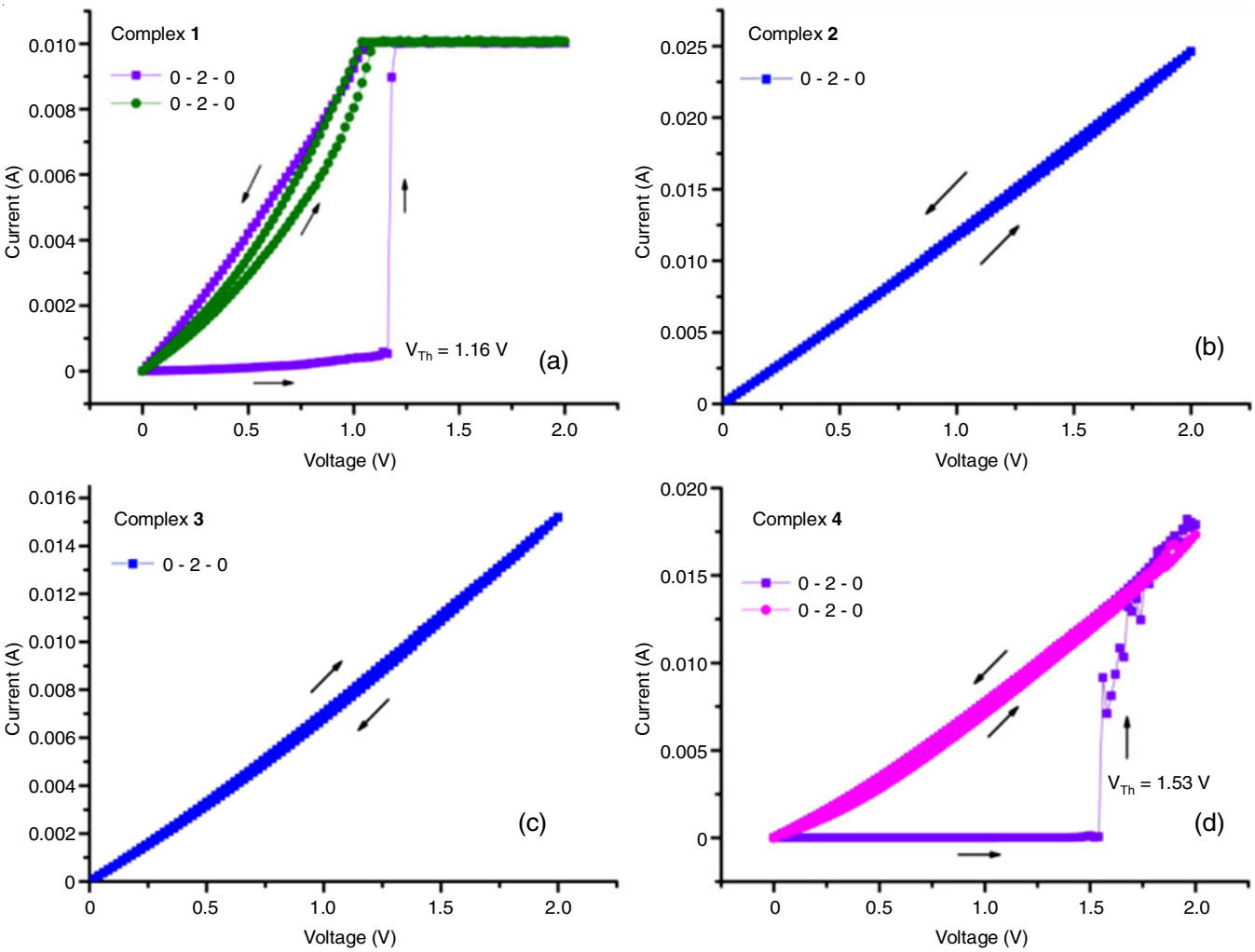

Fig. 7. I-V curves for complex **1** (a), complex **2** (b), complex **3** (c) and complex **4** (d)

tungsten have been designed using four complexes. Herein, the complexes act as the active layer, ITO as bottom electrode and tungsten as top electrode [39,40]. All the four devices have been exposed to electrical biass optimized as 0-2V-0 with no compliance current. Complexes **2** and **3** showed ohmic behaviour with linear curve (Fig. 7), which depicts that the devices are conducting in nature since it followed Ohms Law *i.e.*, $I \infty V$. The highest currents obtained for both the devices were 24.6 and 15.1 mA, respectively. The average resistances obtained throughout the whole bias voltage were 0.0123 Ω and 0.0076 Ω for D2 and D3, respectively.

However, devices with complexes **1** and **4** showed very interesting behaviour. Initially, both the devices remain at low conducting (OFF state) up to a certain voltage, but once it reaches to a threshold value (V_{Th}) the current abruptly increases and then goes to higher current value (ON State). Such phenomenon where the conducting nature of a device changes upon application of certain bias voltage is called resistive switching (RS) [41]. Interestingly, once the devices were at ON state and if a reverse bias (2V→0) is applied the device retains its ON State [42,43]. It has been observed that both the devices can retain their ON state after switching even up to 1000 consecutive scan cycles (0→2→0→2). Such resistive switching has a lot of applications in molecular electronics especially towards designing write once read many memory applications (WORM) [42,44]. Threshold voltage for complex **1** based device was V_{TH1} = 1.16 V and that for complex **4** based device was V_{TH4} = 1.53 V. The observed difference in threshold voltages may be due to difference in structure of the two complexes as well as their organization within the device active layer.

FESEM study: Interestingly, it has been observed that all the four molecules formed nano scale aggregated structure, although the morphology and shape as well as dimension of the aggregated structure were different from each other as observed in the FESEM images (Fig. 8). Complex **1** organizes more or less uniformly, whereas complex **2** formed porous structures within the aggregates. On the other hand, remaining two complexes do not show any specific structures. Observed differences in the aggregated structure of the four complexes may be responsible for the observed differences in optoelectronics behaviour of the four complexes as observed in the earlier studies [45].

Antibacterial activities: The antibacterial activity of all the metal complexes (**1**-**4**) and K_2(*i*-MNT)·H_2O were studied against Gram-negative strain *viz. Escherichia coli* and *Shigella boydii* with standard antibiotic gentamicin was used as a positive control and also studied against Gram-positive strain *Staphylococcus aureus* with standard antibiotic polymyxin B was used as a positive control. Statistical analysis was performed and the differences between groups were examinedby Student's t test. It has been found that the complexes **2**, **4** and K_2(*i*-MNT)·H_2O has no antibacterial activity against strain *Escherichia*

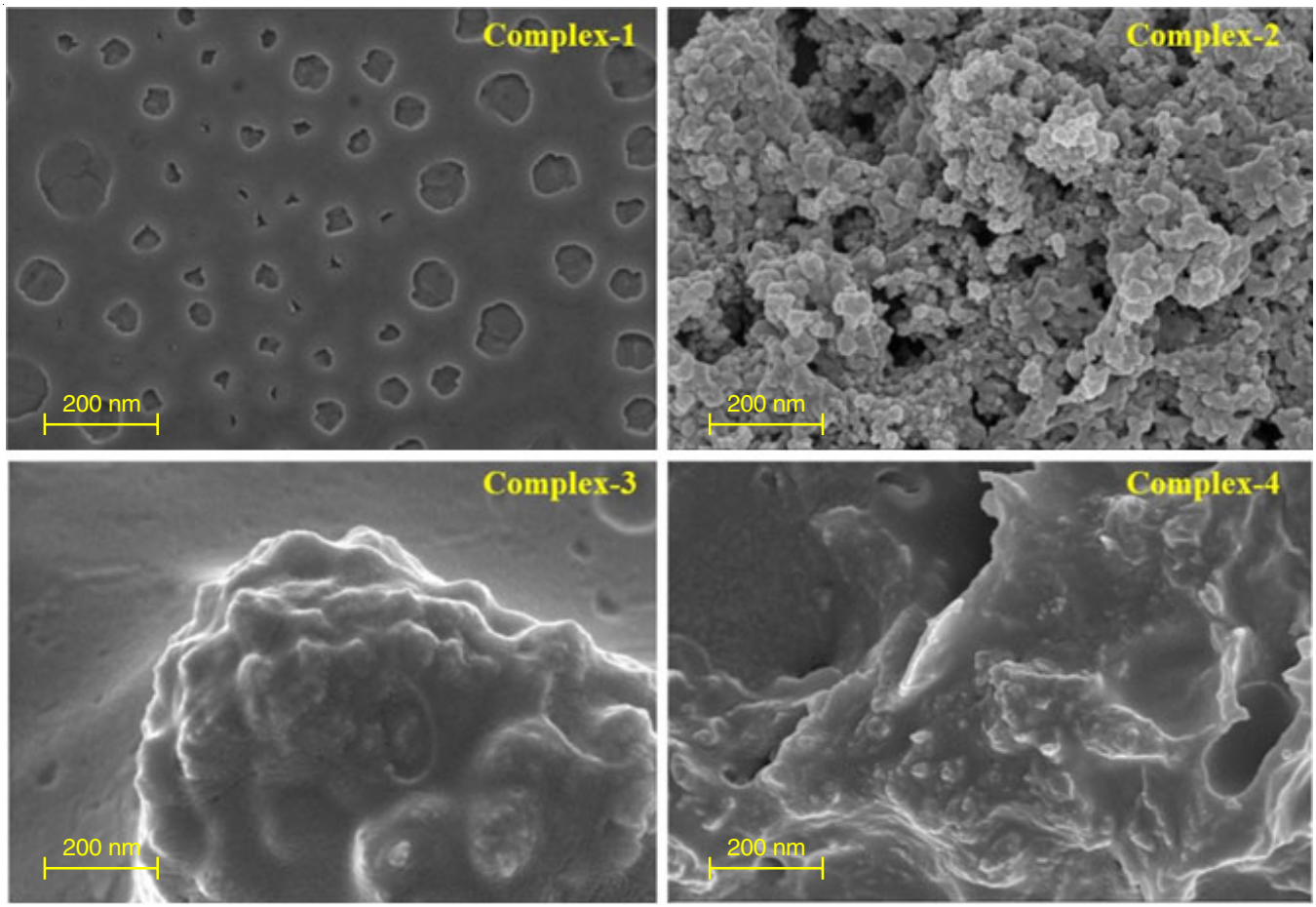

Fig. 8. FESEM images for complexes **1**, **2**, **3** and **4**

coli (Fig. 9). Complex **1** shows significant difference between blank and 100 µg/disc doses but no significant difference has been found between blank and two other doses *i.e.* 1 µg/disc and 10 µg/disc. Complex **3** with100 µg/disc concentration shows most potent antibacterial activity against strain *Escherichia coli* where diameter of zone of inhibition is 17.33 mm. There is highly significant difference between blank and 100 µg/disc dose in complex **3**, which is also statistically equivalent to 100 µg/disc dose of positive control but no significant difference has been found between blank and 1 µg/disc dose in drug complex **3**.

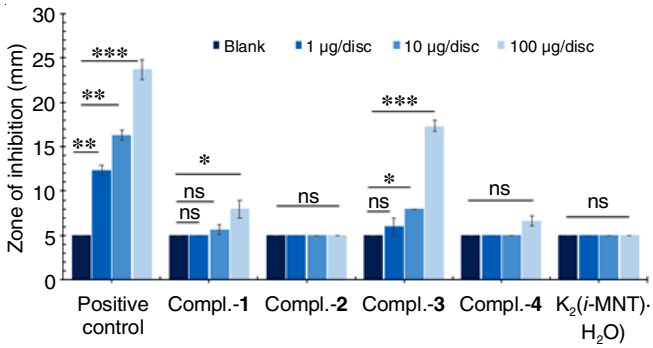

Fig. 9. Zone diameter at different concentration of complexes **1**, **2**, **3**, **4** and $K_2(i\text{-MNT})\cdot H_2O$ against strain *Escherichia coli* (I). The data information is shown as the mean ± standard deviation of three dose concentrations (*$p < 0.05$, **$p < 0.01$, ***$p < 0.001$, ns = no significance $p > 0.05$)

It has been found that complexes **1**, **2** and $K_2(i\text{-MNT})\cdot H_2O$ has no antibacterial activity against strain *S. aureus* (Fig. 10). Complex **3** shows significant difference between blank and

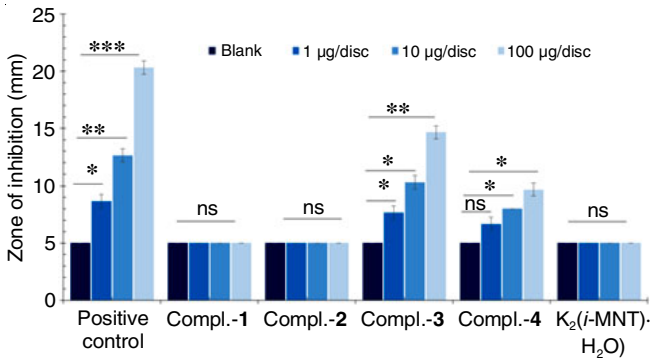

Fig. 10. Zone diameter at different concentration of complexes **1**, **2**, **3**, **4** and $K_2(i\text{-MNT})\cdot H_2O$ against strain *Staphylococcus aureus* (J)

all the 3 doses with highest in between blank and 100 µg/disc dose which is about 14.67 mm whereas complex **4** shows significant difference in between blank and 10 µg/disc dose with zone diameter of 8 mm and between blank and 100 µg/disc dose whose diameter of zone of inhibition is 9.67 mm but no statistical difference has been found between blank and 1 µg/disc dose.

Similarly, complexes **1**, **2** and $K_2(i\text{-MNT})\cdot H_2O$ has no antibacterial activity against strain *Shigella boydii* (Fig. 11). Complex **4** shows statistically significant difference between blank and 100 µg/disc dose with zone diameter of 8 mm but no statistically significant difference has been found in other 2 doses. Complex **3** with 100 µg/disc concentration shows most potent antibacterial activity against strain *Shigella boydii* where diameter of zone of inhibition is 17.67 mm. There is highly significant difference between blank and 100 µg/disc dose in complex **3** which is also statistically equivalent to 100 µg/disc dose of positive control but no significant difference has been found between blank and 1 µg/disc dose.

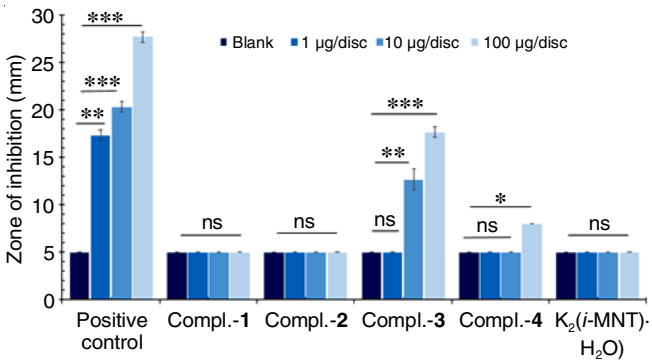

Fig. 11. Zone diameter at different concentration of complexes **1**, **2**, **3**, **4** and $K_2(i\text{-MNT})\cdot H_2O$ against strain *Shigella boydii* (Q)

Among various compounds, complexes **1**, **2** and $K_2(i\text{-MNT})\cdot H_2O$ has no such antibacterial activity against various bacterial strains but complexes **3** and **4** has antibacterial activity with complex **3** being the potent one. The compound is diffused in the agar media and gradually the concentration of compound is decreasing as it goes far from the disc.

Antifungal activities: The synthesized metal(II) complexes and ligand $K_2(i\text{-MNT})\cdot H_2O$ underwent testing against five fungi, with results presented in Table-1, focusing on their minimum inhibitory concentration (MIC). Griseofulvin, the standard sample, exhibited an MIC value of 0.1 mg/mL. The antifungal

TABLE-1
ANTIFUNGAL ACTIVITY OF THE COMPLEXES **1**, **2**, **3**, **4**, $K_2(i\text{-MNT})\cdot H_2O$ AND GRISEOFULVIN

Materials (1 mg/mL)	Minimum inhibitory concentration (mg/mL)				
	M. grisea	*C. miyabeanus*	*S. endobioticum*	*C. albicans*	*T mentagrophytes*
Complex **1**	7(FS)	9(FS)	11(FS)	NA	NA
Complex **2**	8(FS)	10(FC)	9(FS)	NA	NA
Complex **3**	8(FS)	8(FS)	11(FS)	NA	NA
Complex **4**	10(FC)	11(FS)	12(FC)	NA	NA
$K_2(i\text{-MNT})\cdot H_2O$	NA	NA	NA	NA	NA
Control (DMSO)	NA	NA	NA	NA	NA
Griseofulvin (10 µg/disc)	0.1	0.1	0.3	0.2	0.4

All readings were based on 5 replicates ± SEM, (NA) = Not active. FC = Fungicidal, FS = Fungistatic

activity of the synthesized complexes proved significant against *Magnaporthe grisea*, *Cochliobolus miyabeanus* and *Synchitrium endobioticum*. However, it displayed no fungicidal activity against *Candida albicans* and *Trichophyton mentagrophytes*. On the other hand, ligand K_2(*i*-MNT)·H_2O had no significant impact on any of the fungi that were examined. Typically, the coordination of an organic ligand to a metal ion enhances the antifungal activities due to increased lipophilicity. This enhancement makes it easier for complex molecules to cross lipid bilayers, which limits the growth of microbes [46,47]. Metal ions adsorbed onto the surface of microbial cell walls, disrupting the cellular respiration process and impeding protein synthesis, ultimately restraining the growth of microorganisms. The overlapping of ligand and metal ion orbitals leads to the delocalization of π-electrons over the entire chelate ring, intensifying the lipophilicity of the complexes compared to the free ligand [48]. The efficacy of the metal complexes against different fungi depends on the permeability of microbial cell membranes or changes in the ribosomes of microbial cells.

Conclusion

Four new transition metal(II) complexes (**1**-**4**) were synthesized by using metal(II) salts (M = Ni, Co, Cd or Zn) with 1,1-dicyanoethylene-2,2-dithiolate (*i*-MNT^{2-}) and *p*-phenylenediamine (PPD) ligands were characterized by elemental analysis, UV-Vis, IR spectroscopy and NMR spectroscopy. The stoichiometric calculations and UV-Vis transition investigations have led to the proposed octahedral geometry for Ni(II), distorted octahedral for Co(II), tetrahedral geometry for Cd(II) and Zn(II) complexes. The thin films incorporation of all four complexes showed an evident red shift in the absorption maximum, suggesting their successful assembly. Particularly, the luminescence properties display prominent fluorescence within the visible range. The I-V characteristics analysis unveiled that complex **2** and **3** displayed the ohmic behaviour, exhibiting a linear curve. In contrast, complexes **1** and **4** initially maintained a low conducting state (OFF state) until reaching a specific voltage threshold (V_{Th}), at which point the current sharply increased, transitioning to a higher current state (ON state). Examining the FESEM images, the complexes exhibited a distinct nano-scale aggregated structure. In terms of antibacterial activity, complexes **3** and **4** exhibited significant efficacy against various bacterial strains, with complex **3** demonstrating particularly potent effects. All the four complexes demonstrated significant fungicidal activity against *Magnaporthe grisea*, *Cochliobolus miyabeanus* and *Synchitrium endobioticum*.

ACKNOWLEDGEMENTS

The corresponding author, Arijit Das would like to extend gratitude for the financial support received from the SERB, DST, GoI, New Delhi (SERB's Sanction order No. EEQ/2021/000257; dated 25/02/2022).

CONFLICT OF INTEREST

The authors declare that there is no conflict of interests regarding the publication of this article.

REFERENCES

1. M.K. Singh and A.D. Paul, *Transition Met. Chem.*, **30**, 655 (2005); https://doi.org/10.1007/s11243-005-4586-1
2. M.K. Singh, A. Das and B. Paul, *Transition Met. Chem.*, **32**, 732 (2007); https://doi.org/10.1007/s11243-007-0238-y
3. D.L. Long, Y. Cui, J.T. Chen, W.-D. Cheng and J.-S. Huang, *Polyhedron*, **17**, 3969 (1998); https://doi.org/10.1016/S0277-5387(98)00195-8
4. D.L. Long, J.T. Chen, Y. Cui and J.S. Huang, *Chem. Lett.*, **27**, 171 (1998); https://doi.org/10.1246/cl.1998.171
5. X.K. Gao, J.M. Dou, D.C. Li, F.-Y. Dong and D.-Q. Wang, *J. Chem. Crystallogr.*, **35**, 107 (2005); https://doi.org/10.1007/s10870-005-2798-z
6. L.Q. Kong, J.M. Dou, D.-C. Li and D.-Q. Wang, *J. Mol. Struct.*, **785**, 186 (2006); https://doi.org/10.1016/j.molstruc.2005.10.034
7. L. Kong, J. Xu, S. Li, D. Li and J. Dou, *Synth. React. Inorg. Met.-Org. Nano-Met. Chem.*, **46**, 617 (2016); https://doi.org/10.1080/15533174.2014.988803
8. A.-Q. Zhou and C.-L. Ni, *Acta Crystallogr. E Struct. Rep. Online*, **63**, m3084 (2007); https://doi.org/10.1107/S160053680705814X
9. Y. Hou, Q. Huang, H. Zuo and C. Ni, *Acta Crystallogr. Sect. E Struct. Rep. Online*, **63**, m2903 (2007); https://doi.org/10.1107/S1600536807053834
10. X. Chen, D.H. Huang, C.Y. Huang, J.R. Zhou, H.R. Zuo, Q. Huang, Y. Hou, L.L. Yu, L.M. Yang, X.-P. Liu, C.-L. Ni and Q.-J. Meng, *Synth. React. Inorg. Met.-Org. Nano-Met. Chem.*, **39**, 179 (2009); https://doi.org/10.1080/15533170902857999
11. S. Perruchas and K. Boubekeur, *Dalton Trans.*, **16**, 2394 (2004); https://doi.org/10.1039/B408458F
12. P.K. Liao, K.G. Liu, C.S. Fang, C.W. Liu, J.P. Fackler Jr. and Y.-Y. Wu, *Inorg. Chem.*, **50**, 8410 (2011); https://doi.org/10.1021/ic2009896
13. N. Kobayashi, T. Naito and T. Inabe, *Mol. Cryst. Liq. Cryst.*, **376**, 233 (2010); https://doi.org/10.1080/10587250210784
14. M.K. Singh, S. Sutradhar, B. Paul, S. Adhikari, F. Laskar, S. Acharya, D. Chakraborty, S. Biswas, A. Das, S. Roy and A. Frontera, *J. Mol. Struct.*, **1164**, 334 (2018); https://doi.org/10.1016/j.molstruc.2018.03.073
15. S.S. Attar, L. Marchiò, L. Pilia, M.F. Casula, D. Espa, A. Serpe, M. Pizzotti, D. Marinotto and P. Deplano, *New J. Chem.*, **43**, 12570 (2019); https://doi.org/10.1039/C9NJ02976A
16. S. Adhikari, T. Bhattacharjee, A. Das, S. Roy, C.G. Daniliuc, J.K. Zarêba, A. Bauzá and A. Frontera, *CrystEngComm*, **22**, 8023 (2020); https://doi.org/10.1039/D0CE01233E
17. A. Mishra, G.K. Mishra, Anamika, N. Singh, R. Kant and K. Kumar, *Dalton Trans.*, **53**, 1680 (2024); https://doi.org/10.1039/D3DT03932C
18. H. Mehri and Y. Gholiee, *Transition Met. Chem.*, (2024); https://doi.org/10.1007/s11243-024-00579-6
19. M. Mitra, O. Mrózek, M. Putscher, J. Guhl, B. Hupp, A. Belyaev, C.M. Marian and A. Steffen, *Angew. Chem. Int. Ed.*, **63**, e202316300 (2024); https://doi.org/10.1002/anie.202316300
20. R.P. Tang, K.M. Wong, N. Zhu and V.W. Yam, *Dalton Trans.*, **20**, 3911 (2009); https://doi.org/10.1039/b821264c
21. S. Adhikari, T. Bhattacharjee, S. Bhattacharjee, C.G. Daniliuc, A. Frontera, E.M. Lopato and S. Bernhard, *Dalton Trans.*, **50**, 5632 (2021); https://doi.org/10.1039/D1DT00352F
22. M.K. Singh, S. Sutradhar, B. Paul, S. Adhikari, R.J. Butcher, S. Acharya and A. Das, *J. Coord. Chem.*, **67**, 3613 (2014); https://doi.org/10.1080/00958972.2014.972388
23. M.K. Singh, S. Sutradhar, B. Paul, S. Adhikari, R.J. Butcher, S. Acharya and A. Das, *J. Coord. Chem.*, **68**, 1423 (2015); https://doi.org/10.1080/00958972.2015.1013946
24. M.K. Singh, S. Sutradhar, B. Paul, S. Adhikari, R.J. Butcher, S. Acharya and A. Das, *J. Coord. Chem.*, **69**, 168 (2016); https://doi.org/10.1080/00958972.2015.1112004

25. M.K. Singh, S. Sutradhar, B. Paul, S. Adhikari, F. Laskar, R.J. Butcher, S. Acharya and A. Das, *J. Mol. Struct.*, **1139**, 395 (2017); https://doi.org/10.1016/j.molstruc.2017.03.073
26. S. Adhikari, T. Bhattacharjee, R.J. Butcher, M. Porchia, M. De Franco, C. Marzano, V. Gandin and F. Tisato, *Inorg. Chim. Acta*, **498**, 119098 (2019); https://doi.org/10.1016/j.ica.2019.119098
27. T. Bhattacharjee, S. Adhikari, S. Bhattacharjee, S. Debnath, A. Das, C.G. Daniliuc, K. Thirumoorthy, S. Malayaperumal, A. Banerjee, S. Pathak and A. Frontera, *Inorg. Chim. Acta*, **543**, 121157 (2022); https://doi.org/10.1016/j.ica.2022.121157
28. K.A. Jensen, L. Henriksen, O.B. Weeks, U. Schwieter and J. Paasivirta, *Acta Chem. Scand.*, **22**, 1107 (1968); https://doi.org/10.3891/acta.chem.scand.22-1107
29. P. Debnath, P. Debnath M. Roy L. Sieroñ, W. Maniukiewicz, T. Aktar D. Maiti, A.S. Novikov and T.K. Misra, *Crystals*, **12**, 1582 (2022); https://doi.org/10.3390/cryst12111582
30. A. Barry, in eds.: V. Lorian, Antibiotics in Laboratory Medicine, Williams and Wilkins, Baltimore, MD, p. 116 (1991).
31. T. Rosu, M. Negoiu, S. Pasculescu, E. Pahontu, D. Poirier and A. Gulea, *Eur. J. Med. Chem.*, **45**, 774 (2010); https://doi.org/10.1016/j.ejmech.2009.10.034
32. F.A. Cotton, G. Wilkinson, C.A. Murillo and M. Bochmann, Advanced Inorganic Chemistry, John Wiley & Sons, Inc., New York, edn. 6, p. 820 (1999).
33. A.B.P. Lever, Inorganic Electronic Spectroscopy, Elsevier Publishing Company: New York, p. 318 (1968).
34. A.M. El-Mahalawy, R.A. Almotiri, M.M. Alkhamisi and A.R. Wassel, *Surf. Interfaces*, **30**, 101953 (2022); https://doi.org/10.1016/j.surfin.2022.101953
35. P. Debnath, S. Chakraborty, S. Deb, J. Nath, B. Dey, D. Bhattacharjee, H. Soda, M. Tominaga, Y. Suzuki, J. Kawamata and S.A. Hussain, *Appl. Clay Sci.*, **147**, 105 (2017); https://doi.org/10.1016/j.clay.2017.07.013
36. P. Debnath, S. Chakraborty, S. Deb, J. Nath, D. Bhattacharjee and S.A. Hussain, *J. Phys. Chem. C*, **119**, 9429 (2015); https://doi.org/10.1021/acs.jpcc.5b02111
37. J.P. Fackler Jr. and D. Coucouvanis, *J. Am. Chem. Soc.*, **88**, 3913 (1966); https://doi.org/10.1021/ja00969a005
38. M.A. Bellimam, A. Stambouli, N. El Karni, T. Bouayoun and A. El Bouri, *Acta Clin. Belg.*, **61(sup1)**, 41 (2006); https://doi.org/10.1179/acb.2006.068
39. W. Shen, R. Dittmann, U. Breuer and R. Waser, *Appl. Phys. Lett.*, **93**, 222102 (2008); https://doi.org/10.1063/1.3039809
40. B. Dey, S. Sarkar, H. Banik and S. Arshad Hussain, *Mater. Today Proc.*, **46**, 6290 (2021); https://doi.org/10.1016/j.matpr.2020.05.192
41. S. Sarkar, H. Banik, S. Suklabaidya, B. Deb, S. Majumdar, P.K. Paul, D. Bhattacharjee and S.A. Hussain, *Langmuir*, **37**, 4449 (2021); https://doi.org/10.1021/acs.langmuir.0c03629
42. H. Banik, S. Sarkar, D. Bhattacharjee and S.A. Hussain, *ACS Appl. Electron. Mater.*, **3**, 5248 (2021); https://doi.org/10.1021/acsaelm.1c00750
43. F.Y. Rahman, S. Sarkar, H. Banik, M.J. Uddin, D. Bhattacharjee and S.A. Hussain, *Mater. Today Proc.*, **65**, 2693 (2022); https://doi.org/10.1016/j.matpr.2022.05.341
44. R. Paul, H. Banik, M. Alzaid, D. Bhattacharjee and S.A. Hussain, *ACS Omega*, **7**, 17583 (2022); https://doi.org/10.1021/acsomega.1c07395
45. A. Das, S.A. Hussain, H. Banik, D. Maiti, T. Aktar, B. Paul, P. Debnath, L. Sieron, A. Bhattacharya, K.L. Bhowmik, W. Maniukiewicz and P. Debnath, *Polyhedron*, **18**, 116747 (2024); https://doi.org/10.1016/j.poly.2023.116747
46. Y. Anjaneyulu and R.P. Rao, *Synth. React. Inorg. Met.-Org. Chem.*, **16**, 257 (1986); https://doi.org/10.1080/00945718608057530
47. M. Montazerozohori, S. Zahedi, M. Nasr-Esfahani and A. Naghiha, *J. Ind. Eng. Chem.*, **20**, 2463 (2014); https://doi.org/10.1016/j.jiec.2013.10.027
48. N. Dharmaraj, P. Viswanathamurthi and K. Natarajan, *Transition Met. Chem.*, **26**, 105 (2001); https://doi.org/10.1023/A:1007132408648